Inorg. Chem. **2003**, *42*, 8019–8027

Cationic Mn_{12} Single-Molecule Magnets and Their Polyoxometalate Hybrid Salts

Alicia Forment-Aliaga, Eugenio Coronado,* Marta Feliz,† Alejandro Gaita-Ariño, Rosa Llusar,† and Francisco M. Romero*

Instituto de Ciencia Molecular, Universitat de València, 46100-Burjassot, Spain

Received April 17, 2003

A carboxy-substituted alkylammonium salt, namely, (4-carboxybenzyl)tributylammonium hexafluorophosphate, **Z**HPF_6, was prepared and used as incoming carboxylate ligand in a ligand-exchange reaction with $[Mn_{12}O_{12}(O_2CCH_3)_{16}(H_2O)_4]$ (**1**) to afford a new Mn_{12} single-molecule magnet (SMM), $[Mn_{12}O_{12}(\mathbf{Z})_{16}(H_2O)_4][PF_6]_{16}$ (**2**), bearing 16 cationic units appended in the periphery. This compound behaves as a single-molecule magnet, exhibiting an out-of-phase ac magnetic susceptibility χ''_M signal that shows a single maximum in the 3.1–5.4 K temperature range. The frequency dependence of the maximum follows an Arrhenius law, with an effective energy barrier for reorientation of the spins $U_{eff} = 53$ K. The reduced magnetization versus *H*/*T* data at different temperatures were fitted by using a Hamiltonian containing Zeeman, axial, and quartic zero-field splitting terms. The expected spin ground state $S = 10$ was found, and the least-squares fit afforded the following zero-field-splitting parameters: $D = -0.44$ cm^{-1}; $B_4^0 = 0.12 \times 10^{-4}$ cm^{-1}. Magnetization hysteresis loops were observed for **2**, with a coercive field $H_c = 0.34$ T. Complex **2** has been used as countercation in the preparation of a family of hybrid salts containing different polyoxometalate anions, $[Mn_{12}O_{12}(\mathbf{Z})_{16}(H_2O)_4][W_6O_{19}]_8$ (**3**), $[Mn_{12}O_{12}(\mathbf{Z})_{16}(H_2O)_4][PW_{12}O_{40}]_{16/3}$ (**4**), $[Mn_{12}O_{12}(\mathbf{Z})_{16}(H_2O)_4][(H_3O)PW_{11}O_{39}Ni]_4$ (**5**), and $[Mn_{12}O_{12}(\mathbf{Z})_{16}(H_2O)_4][(H_3O)PW_{11}O_{39}Co]_4$ (**6**). **3**–**6** exhibit typical magnetic hysteresis loops with higher coercive fields for the complexes containing diamagnetic polyanions: $H_c = 0.075$ T (**3**), 0.046 T (**4**), 0.016 T (**5**), and 0.0075 T (**6**). However, the dynamics of the magnetic behavior below the blocking temperature is similar in all compounds. Broad frequency-dependent out-of-phase ac susceptibility signals are observed, presumably due to mixtures of different Jahn–Teller isomers. Their temperature dependence is also typical of an activated-energy process, with effective energy barriers in the 50 K range, irrespective of the nature of the polyoxoanion (diamagnetic, as in **3** and **4**, or paramagnetic, as in **5** and **6**). These findings seem to discard any influence of the polyoxometalate in the magnetic properties of the SMM.

Introduction

There is a growing interest in the chemistry and physics of dodecanuclear manganese complexes (Mn_{12}) of formula $[Mn_{12}O_{12}(O_2CR)_{16}(H_2O)_4]$.[1,2] These mixed-valence magnetic clusters contain four Mn(IV) centers ($S = 3/2$ spin) in a central Mn_4O_4 cubane unit and eight Mn(III) centers ($S = 2$ spin) that are exchange-coupled (Figure 1) to give a spin ground state ($S = 10$). The presence of the axially distorted Mn^{3+} ions (Jahn−Teller effect) provides also a source for magnetic anisotropy in the system. A large spin ground state and a significant magnetic anisotropy are the basic ingredients of a single-molecule magnet (SMM). The anisotropy splits in zero field the 21 energy levels corresponding to different M_S ($-10 \le M_S \le 10$), and the energy of each level is given by the expression $E = M_S^2 D$, where D is the axial zero-field-splitting parameter. If D is negative, a potential-energy barrier for reorientation of the spins appears (Figure 2). Below a given temperature (named the blocking temperature), the energy of the barrier is higher than the thermal energy (kT) and the spin of a single molecule can be permanently magnetized in the direction of the applied field.[3] Switching off the field leads to a very slow relaxation of

* To whom correspondence should be addressed. E-mail: fmrm@uv.es (F.M.R.). Phone/fax: +34 963864859.

† Present address: Departament de Ciències Experimentals, Universitat Jaume I, Campus de Riu Sec, P. O. Box 224, Castelló, Spain.

(1) (a) Caneschi, A.; Gatteschi, D.; Sessoli, R.; Barra, A. L.; Brunel, L. C.; Guillot, M. *J. Am. Chem. Soc.* **1991**, *113*, 5873. (b) Sessoli, R.; Tsai, H.-L.; Schake, A. R.; Wang, S.; Vincent, J. B.; Folting, K.; Gatteschi, D.; Christou, G.; Hendrickson, D. N. *J. Am. Chem. Soc.* **1993**, *115*, 1804. (c) Christou, G.; Gatteschi, D.; Hendrickson, D. N.; Sessoli, R. *Mater. Res. Bull.* **2000**, 66.

(2) Gatteschi, D.; Caneschi, A.; Pardi, L.; Sessoli, R. *Science* **1994**, *265*, 1054.

10.1021/ic034407r CCC: $25.00
Published on Web 11/04/2003

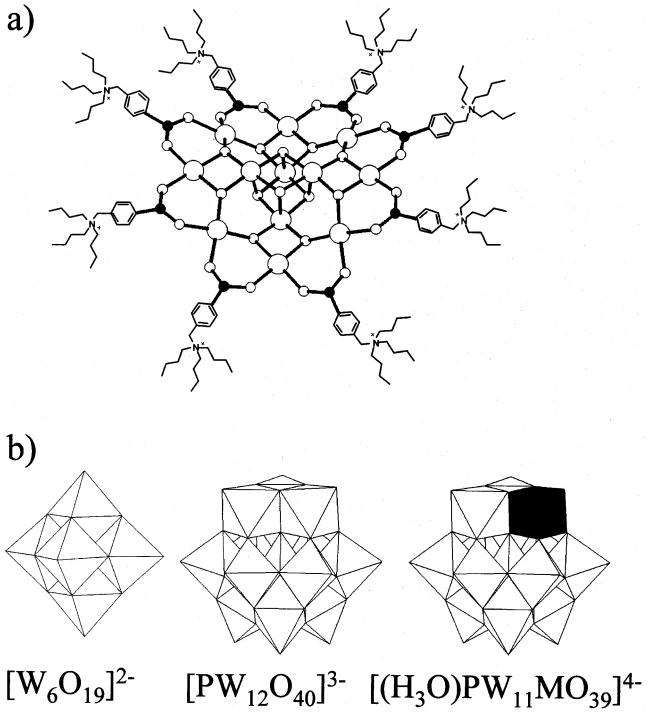

Figure 1. (a) General structural scheme of the $Mn_{12}O_{12}$ core showing the equatorial ammonium-substituted carboxylate ligands. (b) Polyhedral representation of the different polyoxometalates used in this work.

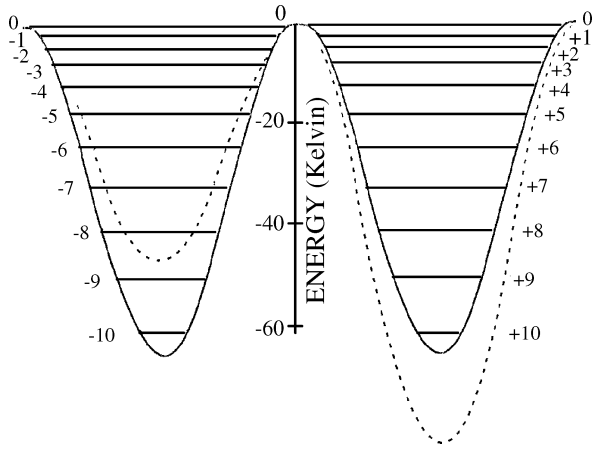

Figure 2. Potential energy diagram for an $S = 10$ spin state with axial symmetry and zero-field splitting. The dotted line shows the double-well potential for the same state in a magnetic field applied along the easy axis.

the magnetization, giving rise to pronounced hysteresis. This observation correlates with the onset of an out-of-phase signal that is frequency-dependent, indicating an energy-activated process. The spin reorientation can also take place by quantum tunneling through the barrier, a phenomenon that has raised a lot of excitement in the physics community as an example of macroscopic quantum tunneling.[4] Also, the magnetic hysteresis of these SMM can be optically monitored by magnetic circular dichroism spectroscopy, providing a rapid method of reading the spin polarization of molecular magnets.[5]

Mn_{12} are neutral but can easily undergo one-electron reduction to the corresponding $[Mn_{12}]^-$ anion.[6,7] It is then possible to combine this anion with functional cationic moieties, like the nitronyl nitroxide radical[8] [*m*-MepyNN]$^+$ or metallocenium cations,[9] and study the influence of the presence of these units in the magnetic behavior of the system. Another strategy for the synthesis of ionic Mn_{12} compounds is based on carboxylate anion-exchange reactions between the acetate precursor, $[Mn_{12}O_{12}(O_2CCH_3)_{16}(H_2O)_4]$ (**1**), and an incoming carboxylate that bears a cation in an appended unit. In this context, we have recently shown that it is possible to synthesize and characterize Mn_{12} bearing quaternary ammonium substituents in the periphery.[10] Functionalization of Mn_{12} magnetic clusters as polycations can favor their self-organization in soft media (LB films) or their deposition as self-assembled monolayers onto polar substrates, like metal oxides or chemically modified metal surfaces. These complexes can be also useful precursors for the preparation of a palette of SMM by simple metathesis reactions. SMM containing magnetic or other functional anions can be envisaged. We are currently interested in the preparation of ionic Mn_{12} that could be combined in hybrid salts with magnetically active ions. Herein we report on the synthesis and magnetic properties of salts containing cationic Mn_{12} and different polyoxoanions.

Experimental Section

Synthesis. All chemicals and solvents were used as received. $[Mn_{12}O_{12}(O_2CCH_3)_{16}(H_2O)_4]$ (**1**),[11] $[N^nBu_4]_2[W_6O_{19}]$,[12a] $[N^nBu_4]_3[PW_{12}O_{40}]$,[12b] $[N^nBu_4]_4[(H_3O)PW_{11}O_{39}Ni]$, and $[N^nBu_4]_4[(H_3O)PW_{11}O_{39}Co]$ were prepared by previously described procedures.[13]

(4-Carboxybenzyl)tributylammonium Bromide, ZHBr. This salt was prepared by a slight modification of the procedure previously reported for the triethylammonium analogue.[14] Yield: 73%. Anal. Found (calcd): C, 59.99 (59.99); H, 9.33 (8.56); N, 3.47 (3.50). ^{1}H NMR (D_2O): δ 8.03 (d, 2H, $J = 8.3$ Hz), 7.54 (d,

(3) Sessoli, R.; Gatteschi, D.; Caneschi, A.; Novak, M. A. *Nature* **1993**, *365*, 141.
(4) (a) Friedman, J.; Sarachik, M.; Tejada, J.; Ziolo, R. *Phys. Rev. Lett.* **1996**, *76*, 3830. (b) Hernández, J.; Zhang, X.; Louis, F.; Bartolomé, J.; Tejada, J.; Ziolo, R. *Europhys. Lett.* **1996**, *35*, 301. (c) Thomas, L.; Lionti, F.; Ballou, R.; Gatteschi, D.; Sessoli, R.; Barbara, B. *Nature* **1996**, *383*, 145.
(5) (a) Cheesman, M. R.; Oganesyan, V. S.; Sessoli, R.; Gatteschi, D.; Thomson, A. J. *Chem. Commun.* **1997**, 1677. (b) McInnes, E. J. L.; Pidcock, E.; Oganesyan, V. S.; Cheesman, M. R.; Powell, A. K.; Thomson, A. J. *J. Am. Chem. Soc.* **2002**, *124*, 9219.
(6) (a) Schake, A. R.; Tsai, H.-L.; de Vries, N.; Webb, R. J.; Folting, K.; Hendrickson, D. N.; Christou, G. *J. Chem. Soc., Chem. Commun.* **1992**, 181. (b) Eppley, H. J.; Tsai, H.-L.; de Vries, N.; Folting, K.; Christou, G.; Hendrickson, D. N. *J. Am. Chem. Soc.* **1995**, *117*, 301. (c) Aubin, S. M. J.; Sun, Z.; Pardi, L.; Krzystek, J.; Folting, K.; Brunel, L.-C.; Rheingold, A. L.; Christou, G.; Hendrickson, D. N. *Inorg. Chem.* **1999**, *38*, 5329.
(7) Soler, M.; Chandra, S. K.; Ruiz, D.; Davidson, E. R.; Hendrickson, D. N.; Christou, G. *Chem. Commun.* **2000**, 2417.
(8) Takeda, K.; Awaga, K. *Phys. Rev. B* **1997**, *56*, 14560.
(9) Kuroda-Sowa, T.; Lam, M.; Rheingold, A. L.; Frommen, C.; Reiff, W. M.; Nakano, M.; Yoo, J.; Maniero, A. L.; Brunel, L. C.; Christou, G.; Hendrickson, D. N. *Inorg. Chem.* **2001**, *40*, 6469.
(10) Coronado, E.; Feliz, M.; Forment-Aliaga, A.; Gómez-García, C. J.; Llusar, R.; Romero, F. M. *Inorg. Chem.* **2001**, *40*, 6084.
(11) Lis, T. *Acta Crystallogr. B* **1980**, *36*, 2042.
(12) (a) Fournier, M. *Inorg. Synth.* **1990**, *27*, 80. (b) Bailar, J. C. *Inorg. Synth.* **1990**, *27*, 132.
(13) Galán-Mascarós, J. R.; Giménez-Saiz, C.; Triki, S.; Gómez-García, C. J.; Coronado, E.; Ouahab, L. *Angew. Chem., Int. Ed. Engl.* **1995**, *34*, 1460.
(14) Lu, M. Y.; Bao, R.; Liu, W.; Li, Y. *J. Org. Chem.* **1995**, *60*, 5341.

2H, $J = 8.3$ Hz), 4.46 (s, 2H), 3.09 (m, 6H), 1.73 (m, 6H), 1.29 (m, 6H, $J = 7.4$ Hz), 0.88 (t, 9H, $J = 7.4$ Hz). IR (KBr, cm^{-1}): 2965 (s), 2876 (s), 2578 (w), 1716 (s), 1471 (m), 1375 (m), 1221 (s), 1183 (s), 1112 (m), 874 (m),830 (m), 737 (m), 641 (m), 587 (w), 513 (w), 465 (w).

(4-Carboxybenzyl)tributylammonium Hexafluorophosphate, ZHPF$_6$. **Z**HBr (8.7 g, 21.8 mmol) was dissolved in the minimum amount of hot water, and the mixture was filtered to remove an insoluble residue. The solution was slowly added over a stirred water solution of KPF_6 (8 g, 43.4 mmol). A white fine powder precipitated. The product was extracted with CH_2Cl_2, the organic phase was dried over $MgSO_4$, and the solvent was evaporated to obtain a white solid. Yield: 70%. Anal. Found (calcd): C, 51.47 (51.61); H, 7.39 (7.36); N, 3.12 (3.01). ^{1}H NMR (CD_3CN): δ 8.10 (d, 2H, $J = 8.3$ Hz), 7.55 (d, 2H, $J = 8.3$ Hz), 4.40 (s, 2H), 3.04 (m, 6H), 1.75 (m, 6H), 1.36 (m, 6H, $J = 7.4$ Hz), 0.99 (t, 9H, $J = 7.35$ Hz). IR (KBr, cm^{-1}): 2967 (s), 2880 (m), 2675 (w), 2552 (w), 1699 (s), 1478 (m), 1428 (m), 1294 (m), 1189 (m), 1127 (m), 842 (s), 737 (m), 558 (s).

[Mn$_{12}$O$_{12}$(Z)$_{16}$(H$_2$O)$_4$][PF$_6$]$_{16}$ (2). $ZHPF_6$ (1.9 g, 4 mmol) was added to a suspension of **1** (0.25 g, 0.125 mmol) in 25 mL CH_2Cl_2. The mixture was stirred overnight, and then it was filtered and the solvent was evaporated under reduced pressure. After addition of toluene, the solution was evaporated to dryness to remove the acetic acid as the toluene azeotrope. This treatment was repeated two times. The product was then taken up in CH_2Cl_2 (25 mL) and treated again with an excess of **Z**HPF$_6$ acid. The entire process was repeated. Finally the product was dissolved in 25 mL of CH_2Cl_2 and absolute EtOH (50 mL) was added. The mixture was kept for a few days at room temperature to obtain a precipitate that was filtered out and washed with absolute EtOH and ether. Yield: 79%. IR (KBr, cm^{-1}): 2967 (s), 2879 (m), 1617 (m), 1560 (w), 1420 (s) 838 (s), 663 (w), 616 (w), 558 (s). Anal. Found (calcd): C, 46.59 (46.01); H, 6.56 (6.47); N, 2.70 (2.68).

[Mn$_{12}$O$_{12}$(Z)$_{16}$(H$_2$O)$_4$][W$_6$O$_{19}$]$_8$ (3). $[N^nBu_4]_2[W_6O_{19}]$ (142 mg, 75 μmol) was dissolved in CH_3CN (10 mL). A solution of **2** (60 mg, 7.2 μmol) in CH_3CN (6 mL) was added dropwise to the above solution, and a brown product precipitated. The mixture was stirred for 10 min, and the solid was separated by centrifugation, thoroughly washed with CH_3CN, and dried under vacuum. IR (KBr, cm^{-1}): 2964 (m), 2875 (w), 1715 (w), 1556 (m), 1416 (s), 1186 (w), 977 (s), 873 (w), 814 (s), 664 (w), 586 (m), 446 (s). Anal. Found (calcd): C, 22.90 (22.23); H, 3.30 (3.12); N, 1.39 (1.30).

[Mn$_{12}$O$_{12}$(Z)$_{16}$(H$_2$O)$_4$][PW$_{12}$O$_{40}$]$_{16/3}$ (4). A similar method used for the synthesis of **3** was employed, starting from $[N^nBu_4]_3[PW_{12}O_{40}]$ (207 mg, 57 μmol). IR (KBr, cm^{-1}): 2961 (m), 2873 (w), 1597 (m), 1475 (w), 1419 (m), 1079 (s), 977 (s), 896 (s), 815 (s), 520 (m). Anal. Found (calcd): C, 18.54 (17.98); H, 3.03 (2.53); N, 1.32 (1.05).

[Mn$_{12}$O$_{12}$(Z)$_{16}$(H$_2$O)$_4$][(H$_3$O)PW$_{11}$O$_{39}$Ni]$_4$ (5). The method used for the synthesis of **3** was employed, starting from $[N^nBu_4]_4[(H_3O)PW_{11}O_{39}Ni]$ (170 mg, 45 μmol). IR (KBr, cm^{-1}): 2961 (m), 2873 (w), 1596 (m), 1477 (w), 1419 (m), 1063 (s), 957 (s), 888 (s), 815 (s), 513 (w). Anal. Found (calcd): C, 23.06 (22.54); H, 3.83 (3.24); N, 1.71 (1.31).

[Mn$_{12}$O$_{12}$(Z)$_{16}$(H$_2$O)$_4$][(H$_3$O)PW$_{11}$O$_{39}$Co]$_4$ (6). A similar method used for the synthesis of **3** was employed, starting from $[N^nBu_4]_4[(H_3O)PW_{11}O_{39}Co]$ (170 mg, 45 μmol). IR (KBr, cm^{-1}): 2961 (m), 2873 (w), 1596 (m), 1556 (w), 1477 (w), 1392 (m), 1061 (s), 958 (s), 885 (s), 809 (s), 515 (w). Anal. Found (calcd): C, 22.99 (22.53); H, 3.59 (3.24); N, 1.58 (1.31).

Compounds **2**−**6** have been obtained and characterized as powders. Following the suggestions of the reviewers, we have compiled the different attempts to grow single crystals (see Supporting Information).

Physical Measurements. Solid-state magic-angle-spinning (MAS) ^{31}P NMR spectra were recorded on a Bruker AV 400 spectrometer (161.9 MHz) using a Doty XC4 double-resonance probe. The spinning frequency was varied in the range 9−11.5 KHz. A decoupling frequency of 376.3 MHz was used for the $^{31}P\{^{19}F\}$ experiments. All spectra were recorded as ground powders at 25 °C. Chemical shifts are reported relative to the ^{31}P resonance in aqueous H_3PO_4 as an external standard.

ESI mass spectra were recorded on either a Micromass Quattro LC instrument or a Waters ZQ mass spectrometer using nitrogen as drying and nebulizing gas. The latter equipment was calibrated with appropriate standard samples.

All the magnetic measurements were done on powder samples with a magnetometer (Quantum Design MPMS-XL-5) equipped with a squid sensor. Variable-temperature susceptibility measurements were carried out in the temperature range 2−300 K in a magnetic field of 0.1 T. The susceptibility data were corrected from the diamagnetic contributions of the salts as deduced by using a Pascal constants table. The ac measurements were performed in the temperature range 2−10 K at different frequencies with an oscillating magnetic field of 0.395 mT. The magnetization data were collected in the $H = 0-5$ T field range at different temperatures between 2 and 5 K.The hysteresis studies were performed between 5 and −5 T, at 2 K, cooling the samples at zero field.

IR transmission measurements of pressed KBr pellets were recorded at room temperature with a Nicolet Avatar 320 FT-IR spectrophotometer in the range 4000−400 cm^{-1}.

CHN elemental analysis was carried out in a CE instruments EA 1110 CHNS analyzer.

Results and Discussion

Synthesis and Characterization. A carboxy-substituted tributylammonium compound was prepared as a bromide salt (**Z**HBr) by alkylation of tributylamine with methyl (4-bromomethyl)benzoate and subsequent hydrolysis of the ester intermediate (Scheme 1a).[14] **Z**HBr is not soluble in common organic solvents but can be converted to the hexafluorophosphate salt (**Z**HPF$_6$) by simple metathesis. The latter was used as incoming acid in the ligand-exchange reaction with the acetate precursor **1** to afford the hexafluorophosphate salt of the polycationic dodecanuclear manganese complex **2**. The final hybrid polyoxometalate-based Mn_{12} compounds (**3**−**6**) precipitated by treatment of **2** with the corresponding tetrabutylammonium polyoxometalate in acetonitrile (Scheme 1b).

Compounds **2**−**6** were characterized in the solid state by ^{31}P MAS NMR spectroscopy. The ^{31}P MAS NMR spectrum of **2** exhibits (Figure 3a) a resonance multiplet centered at −144 ppm. The multiplet is characteristic of hexafluorophosphate anions and consists of seven equally spaced resonance lines due to spin−spin coupling with the ^{19}F ($S = 1/2$) nuclei. Other multiplets are observed at equally spaced intervals of 11 500 Hz, the spinning frequency of the experiment. These are assigned to spinning sidebands. Under ^{19}F decoupling, the multiplets disappear and a sharp signal remains at −144 ppm. Compound **4** exhibits a main resonance line at −15 ppm, with spinning sidebands shifted 9000 Hz at higher and lower field values (Figure 3b). These

Scheme 1. Synthesis of the Polycationic Single-Molecule Magnets

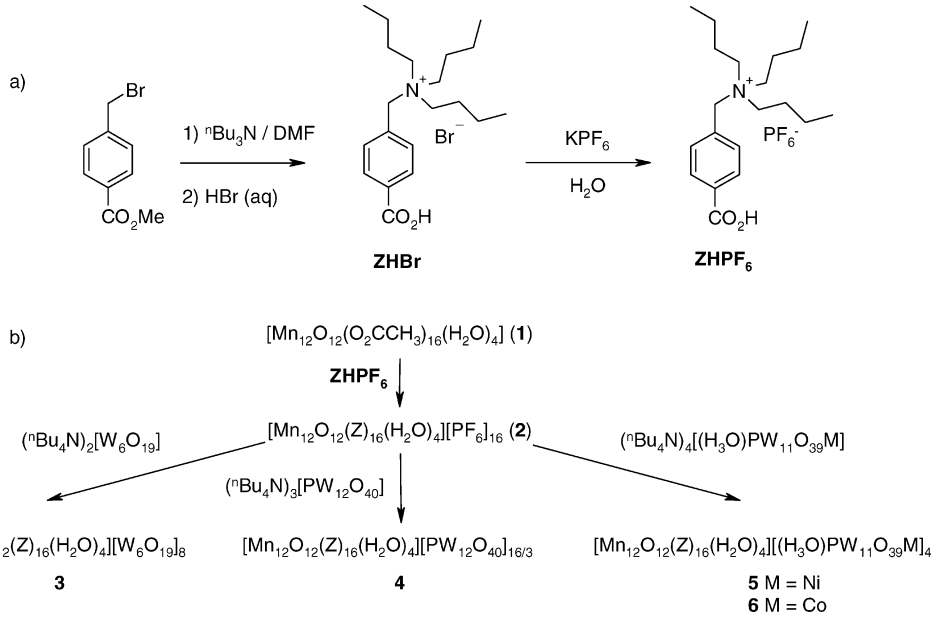

lines do not change under ^{19}F decoupling, and they can be attributed to the Keggin $[PW_{12}O_{40}]^{3-}$ anion. Interestingly, the spectra of **2** and **4** do not show a significant broadening due to the strong paramagnetism of the Mn_{12} polycation. On the contrary, the nickel(II)-containing compound **5** exhibits a broad band centered at −833 ppm. In this case, the paramagnetic center is located at a distance shorter enough to induce an increase of the ^{31}P nuclear spin relaxation. As expected, **6** (with a cobalt(II) center inducing even a higher rate of relaxation) and **3** (without any source of phosphorus) are silent samples.

The soluble precursors **1** and **2** were characterized in solution by electrospray ionization mass spectrometry (ESI-MS). ESI-MS is a soft-ionization technique that is well suited for the analysis of ionic compounds and provides an accurate determination of the molecular mass of relatively large and fragile molecules.[15] Along with the very important applications in proteomics,[16] the technique has also entered the field of inorganic chemistry and offers a good characterization of metallic clusters and polynuclear metal complexes.[17] $[Mn_{12}O_{12}(O_2CR)_{16}(H_2O)_4]$ compounds are neutral, but they can easily undergo reduction processes to form multiply charged anionic species. Electron transfer processes are likely to occur in the ESI source, in such a way that neutral Mn_{12} species can be reduced in situ and detected as anions in the negative mode. Figure 4 shows the ESI-MS (negative mode) analysis of a solution of **1** in CH_3CN. The most intense peak appears at 1795 Da and corresponds to the reduced species $[Mn_{12}O_{12}(O_2CCH_3)_{16}]^-$. Fragmentation of this entity by successive loss of acetate ligands is accompanied by one-electron reduction to give peaks at 1736 and 1677 Da. A signature for a doubly reduced species of the type $[Mn_{12}O_{12}(O_2CCH_3)_{16}]^{2-}$ is present at 897 Da. The charge of each species present in the spectrum has been unambiguously characterized by single ion recording (SIR) at the highest resolution of the spectrometer. Figure 5 shows the experimental and calculated isotopic distributions of the one- and

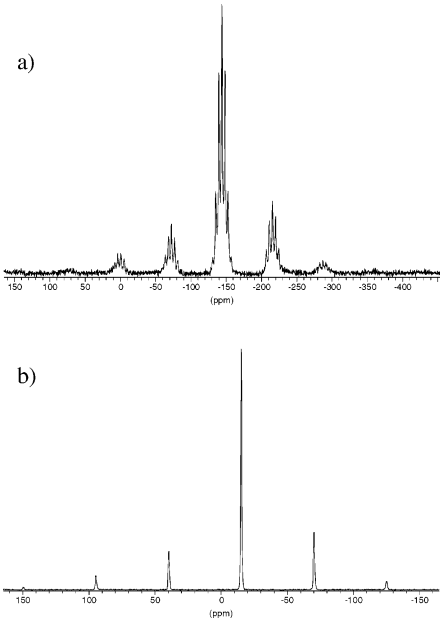

Figure 3. ^{31}P MAS NMR spectra of **2** (a) and **4** (b).

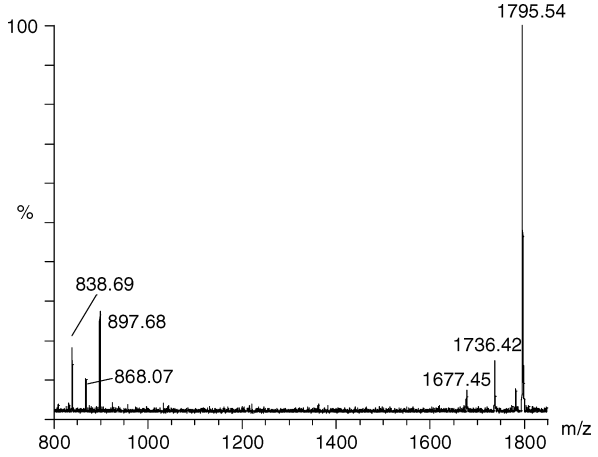

Figure 4. ES-MS (negative mode) spectrum of **1** in acetonitrile. Cone voltage: −25 V.

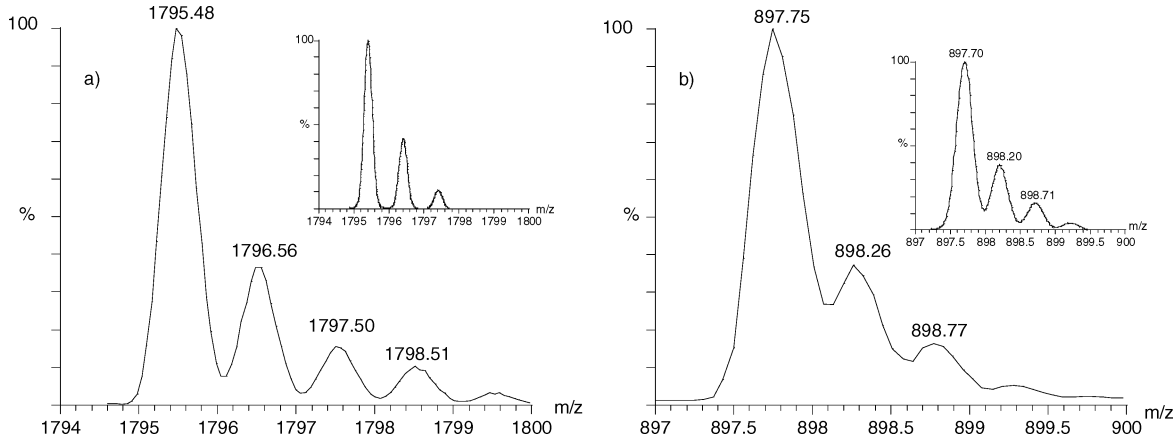

Figure 5. Single-ion recording (SIR) of the one-electron- (a) and two-electron-reduced (b) $[Mn_{12}O_{12}(O_2CCH_3)_{16}]^{n-}$ species. Solvent: CH_3CN. Cone voltage: −25 V (a); −15 V (b).

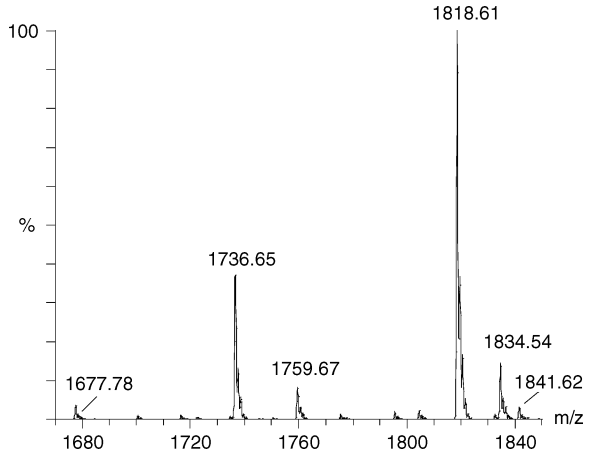

Figure 6. ES-MS (positive mode) spectrum of **1** in acetonitrile. Cone voltage: 50 V.

two-electron-reduced products. As expected for the species that bears a −2 negative charge, the isotopic pattern reveals peaks that are separated by 0.5 Da, whereas the separation between peaks in the isotopic pattern of the most intense peak is 1 Da.

Characterization of **1** is also possible in the positive mode (Figure 6). Interestingly, the main peaks correspond to species in which the neutral core, $[Mn_{12}O_{12}(O_2CCH_3)_{16}]$, has remained intact. These are charged and detected in the positive mode by combination with potassium and/or sodium ions, presumably present as traces in the solutions undergoing electrospray ionization. Again, the nature of the signals has been confirmed by comparing the measured isotopic pattern to that obtained by modeling. Loss of acetate ligands accounts for the presence of other minor peaks. These fragmentations are favored at high cone voltages. Assignments of the different peaks observed in the spectra are gathered in Tables S1 and S2 (see Supporting Information).

The polycationic Mn_{12} molecule **2** has also been characterized by ESI-MS in the positive mode. The compound ionizes readily by successive loss of hexafluorophosphate anions and subsequent one-electron reduction. This results in a series of signals corresponding to cations of the type $[[Mn_{12}O_{12}(\mathbf{Z})_{16}](PF_6)_{16-q}]^{(q-1)+}$ (with charges $q - 1 = 3-6$). The separation Δ between two peaks, P_{q-1} and P_q, of charges $q - 1$ and q, respectively, matches exactly the one obtained with the formula $\Delta = (P_q + M_{PF_6^-})/(q - 1)$, $M_{PF_6^-}$ being the molecular mass of the hexafluorophosphate anion. This provides an unambiguous determination of the mass and charge that corresponds to each signal, even if the resolution of the different isotopic patterns was not possible with our quadrupole spectrometer. Each $[[Mn_{12}O_{12}(\mathbf{Z})_{16}](PF_6)_{16-q}]^{(q-1)+}$ species can be fragmented by loss of carboxylate $\mathbf{Z}PF_6$ anions and one-electron reduction to give a series of peaks with the same charge $[[Mn_{12}O_{12}(\mathbf{Z})_n](PF_6)_{n-q}]^{(q-1)+}$ that are separated by an amount $\delta = M\mathbf{Z}_{PF_6^-}/(q - 1)$. The resulting spectrum is shown in Figure 7. The peak at higher *m*/*z* ratio (2567 Da) corresponds to $[[Mn_{12}O_{12}(\mathbf{Z})_{16}](PF_6)_{12}]^{3+}$. Successive loss of $\mathbf{Z}PF_6$ anions gives peaks at 2412 and 2257 Da. The mass range between 1600 and 1900 Da (Figure 7b) is dominated by the presence of tetrapositive ions derived from a $[[Mn_{12}O_{12}(\mathbf{Z})_{16}](PF_6)_{10}]^{4+}$ fragment, while the 1100−1500 Da region of the spectrum corresponds to penta- and hexapositive ions. Significant values corresponding to the different pseudomolecular peaks are given in Table 1. Interestingly, in some cases, formation of adducts with the free acid can also be detected.

ESI-MS is also a valuable method for monitoring the course of the ligand-exchange reaction. Treatment of **1** with an excess of $\mathbf{Z}HPF_6$ yields a distribution of products of the type $[Mn_{12}O_{12}(O_2CCH_3)_{16-n}(\mathbf{Z})_n](PF_6)_n$ ($n = 13-15$) (Table S3; see Supporting Information). The mixture can be precipitated and retreated with $\mathbf{Z}HPF_6$ to afford a completely substituted compound containing a small amount of the $n = 15$ derivative (peaks marked with an asterisk in Figure 7).

Direct Current Magnetization Studies. Variable-temperature dc magnetic susceptibility data (Figure 8) were measured on complexes **2**−**6** in the 2−300 K range with a 1 kG applied field. For compounds **2**−**4**, the temperature

(15) (a) Hofstadler, S. A.; Bakhtiar, R.; Smith, R. D. *J. Chem. Educ.* **1996**, *73*, A82. (b) Fenn, J. B. Mann, M.; Meng, C. K.; Wong, S. F.; Whitehouse, C. M. *Science* **1989**, *246*, 64. (c) Jardine, I. *Nature* **1990**, *345*, 747.
(16) Yates, J. R., III. *J. Mass. Spectrom.* **1998**, *33*, 19.
(17) Johnson, B. F. G.; McIndoe, J. S. *Coord. Chem. Rev.* **2000**, *200*−*202*, 901.

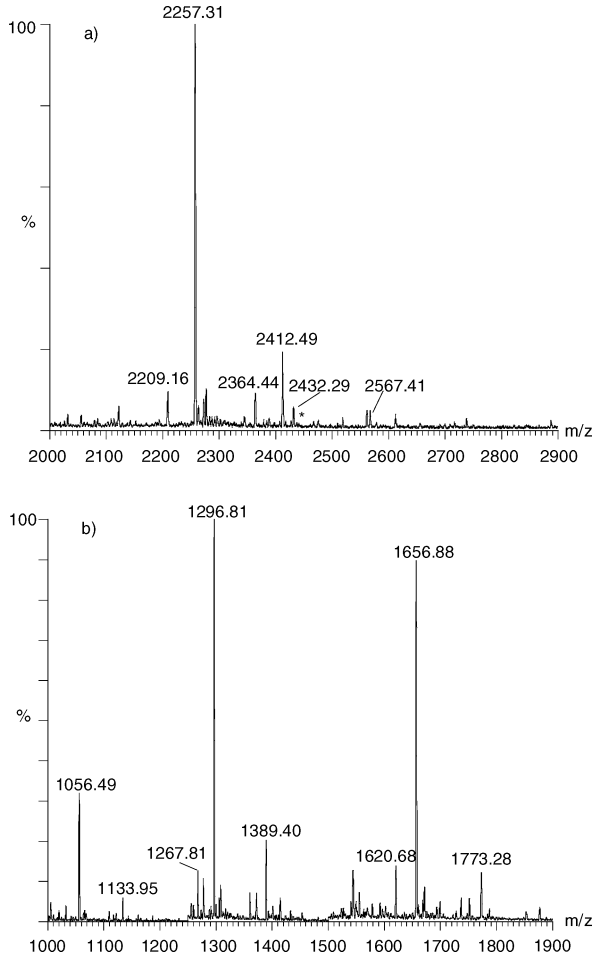

Figure 7. ES-MS (positive mode) spectrum of $[Mn_{12}O_{12}(\mathbf{Z})_{16}](PF_6)_{16}$ in CH_3CN. Cone voltage: 20 V. High-mass (a) and low-mass (b) regions are plotted separately for the sake of clarity.

dependence of the χT product is similar to that previously observed in other Mn_{12} derivatives with $S = 10$ ground state, showing a nearly constant value of 17−22 emu K mol^{-1} at 300 K with a slight decrease on cooling in the 300−150 K temperature range. On further cooling, χT increases rapidly to reach a maximum of 45−50 emu K mol^{-1}, indicating the presence of a large-spin ground state. The temperature of the maximum (10 K) is the same for the three compounds. The steep decrease observed at lower temperatures is basically due to zero-field-splitting (ZFS) effects. The thermal variation of the χT product of **5** shows similar temperature dependence with values that are higher than in the preceding series due to the contribution of the four paramagnetic Ni(II) centers ($S = 1$). It decreases smoothly from 25.8 emu K mol^{-1} at 300 K to 24.3 emu K mol^{-1} at 172 K, then increases to reach a maximum at 14 K, where $\chi T = 55$ emu K mol^{-1}, and falls down at lower temperatures. The cobalt-containing heteropolyanion (**6**) exhibits also similar magnetic properties. The χT product equals 33 emu K mol^{-1} at 300 K. With subtraction of the signal observed for the Keggin derivative **4**, a contribution of 3.1 emu K mol^{-1}/anion is found, which is a reasonable value for an isolated Co(II) center. After a small decrease on cooling to a value of 31.4 emu K mol^{-1} at 172 K, χT increases until a maximum value of 54 emu K mol^{-1} is observed at 9 K. This corresponds to a contribution

Table 1. Pseudomolecular Peaks in the ESI-MS Spectrum of $[Mn_{12}O_{12}(\mathbf{Z})_{16}](PF_6)_{16}$ in CH_3CN[a]

charge (z)	fragment	calcd (m/z)	found (m/z)
+6	$Mn_{12}O_{12}(\mathbf{Z})_{16}(PF_6)_8$ (+2e$^-$)	1186.50	1186.79
+6	$Mn_{12}O_{12}(\mathbf{Z})_{15}(CH_3CO_2)(PF_6)_8$ (+1e$^-$)	1143.12	1143.71
+6	$Mn_{12}O_{12}(\mathbf{Z})_{15}(PF_6)_8$ (+2e$^-$)	1133.28	1133.95
+6	$Mn_{12}O_{12}(\mathbf{Z})_{15}(PF_6)_7$ (+3e$^-$)	1109.12	1109.77
+6	$Mn_{12}O_{12}(\mathbf{Z})_{14}(CH_3CO_2)(PF_6)_7$ (+2e$^-$)	1065.75	1066.12
+6	$Mn_{12}O_{12}(\mathbf{Z})_{14}(PF_6)_7$ (+3e$^-$)	1055.91	1056.49
+6	$Mn_{12}O_{12}(\mathbf{Z})_{14}(PF_6)_6$ (+4e$^-$)	1031.75	1032.11
+5	$Mn_{12}O_{12}(\mathbf{Z})_{15}(CH_3CO_2)(PF_6)_9$ (+1e$^-$)	1400.73	1401.19
+5	$Mn_{12}O_{12}(\mathbf{Z})_{15}(PF_6)_9$ (+2e$^-$)	1388.93	1389.40
+5	$Mn_{12}O_{12}(\mathbf{Z})_{15}(PF_6)_8$ (+3e$^-$)	1359.94	1360.53
+5	$Mn_{12}O_{12}(\mathbf{Z})_{14}(CH_3CO_2)(PF_6)_8$ (+2e$^-$)	1307.89	1308.28
+5	$Mn_{12}O_{12}(\mathbf{Z})_{14}(PF_6)_8$ (+3e$^-$)	1296.08	1296.81
+5	$Mn_{12}O_{12}(\mathbf{Z})_{14}(PF_6)_7$ (+4e$^-$)	1267.09	1267.81
+4	$Mn_{12}O_{12}(\mathbf{Z})_{16}(PF_6)_{10}$ (+2e$^-$)	1852.21	1852.65
+4	$Mn_{12}O_{12}(\mathbf{Z})_{15}(CH_3CO_2)(PF_6)_{10}$ (+1e$^-$)	1787.15	1787.04
+4	$Mn_{12}O_{12}(\mathbf{Z})_{15}(PF_6)_{10}$ (+2e$^-$)	1772.40	1773.28
+4	$Mn_{12}O_{12}(\mathbf{Z})_{15}(PF_6)_9$ (+3e$^-$)	1736.16	1737.02
+4	$Mn_{12}O_{12}(\mathbf{Z})_{14}(CH_3CO_2)(PF_6)_9$ (+2e$^-$)	1671.10	1671.66
+4	$Mn_{12}O_{12}(\mathbf{Z})_{14}(PF_6)_9$ (+3e$^-$)	1656.35	1656.88
+4	$Mn_{12}O_{12}(\mathbf{Z})_{14}(PF_6)_8$ (+4e$^-$)	1620.11	1620.68
+3	$Mn_{12}O_{12}(\mathbf{Z})_{16}(PF_6)_{12}$ (+1e$^-$)	2566.26	2567.41
+3	$Mn_{12}O_{12}(\mathbf{Z})_{16}(PF_6)_{11}$ (+2e$^-$)	2517.94	2518.65
+3	$Mn_{12}O_{12}(\mathbf{Z})_{15}(CH_3CO_2)(PF_6)_{11}$ (+1e$^-$)	2431.19	2432.29
+3	$Mn_{12}O_{12}(\mathbf{Z})_{15}(PF_6)_{11}$ (+2e$^-$)	2411.52	2412.49
+3	$Mn_{12}O_{12}(\mathbf{Z})_{15}(PF_6)_{10}$ (+3e$^-$)	2363.20	2364.44
+3	$Mn_{12}O_{12}(\mathbf{Z})_{14}(CH_3CO_2)(PF_6)_{10}$ (+2e$^-$)	2276.46	2277.49
+3	$Mn_{12}O_{12}(\mathbf{Z})_{14}(PF_6)_{10}$ (+3e$^-$)	2256.78	2257.31
+3	$Mn_{12}O_{12}(\mathbf{Z})_{14}(PF_6)_9$ (+4e$^-$)	2208.46	2209.16

[a] Cone voltage: 20 V, positive mode.

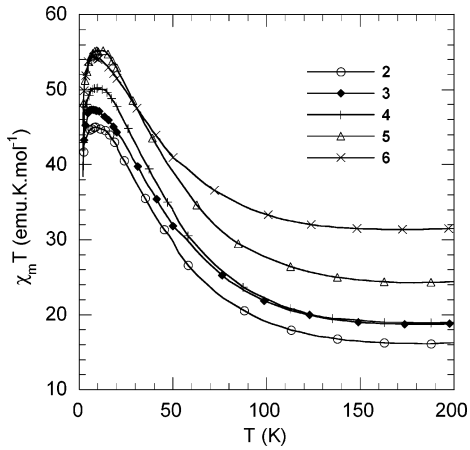

Figure 8. Temperature dependence of the χT product for compounds **2**−**6**.

of 1 emu K mol^{-1}/anion, indicating that the Co^{2+} cations are in their Kramers doublet ground state at low temperatures.

For an understanding of the magnetism of the Mn_{12} polycation in the different salts, it is necessary to determine the main features of the spin Hamiltonian that governs the system, like the value of the spin in the ground state and the magnitude of the different magnetic parameters. With this purpose in mind, magnetization data were collected for **2**−**4** in the $H = 0.5$−5 T field range at different temperatures between $T = 2$ and 5 K. Compounds **5** and **6** were not included in this study, as they bear an additional magnetic contribution of the counteranions that cannot be easily subtracted with enough accuracy to yield quantitative results. Figure 9 shows the dependence of the reduced magnetization ($M/N\mu_B$) of **2**−**4** on the ratio H/T, where N is the Avogadro

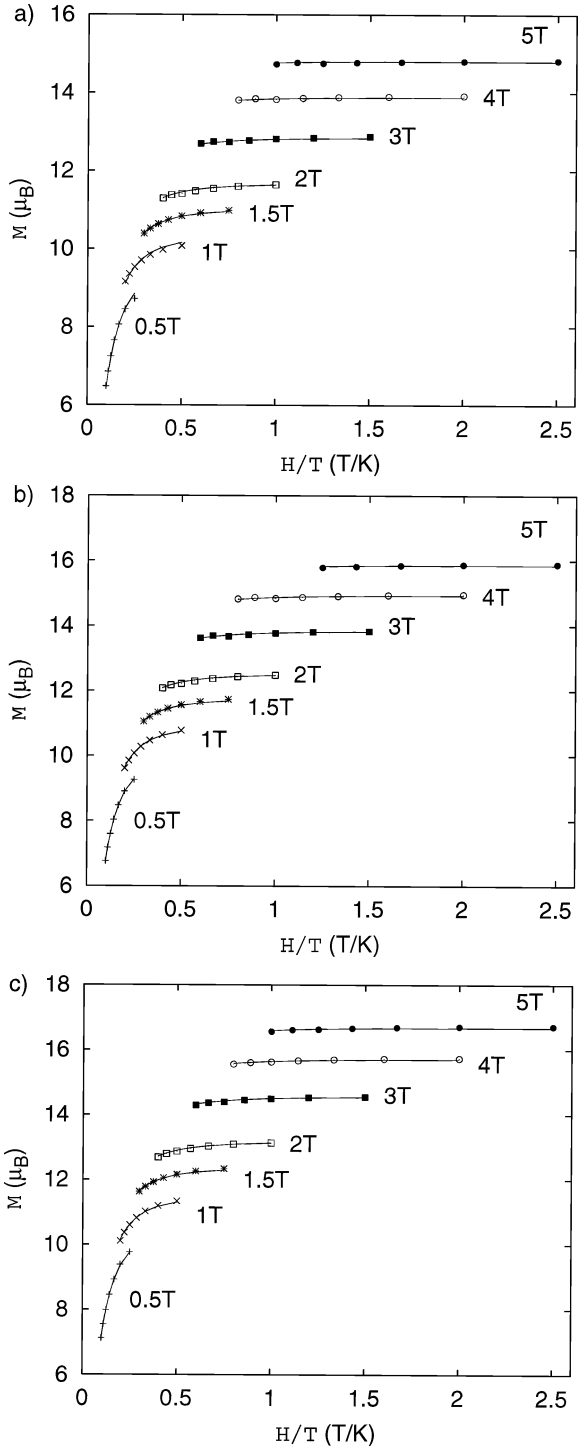

Figure 9. Plots of reduced magnetization versus H/T for **2** (a), **3** (b), and **4** (c) at the indicated applied fields. The isofield lines are least-squares fits to the data according to eqs 2 and 3. See Table 2 for the fit parameters.

number and μ_B is the Bohr magneton. Assuming that the ground state is the only populated state in the range of temperatures studied, the magnetization curve should follow a Brillouin law and the various isofield lines should be superimposed with a saturation value equal to gS. This is clearly not the case in these compounds. The absence of a univocal correspondence between the reduced magnetization and the H/T ratio indicates that the ground state is split by an axial ZFS, as has been pointed out in the study of other

Table 2. Magnetic Parameters for **2**−**6**

compd	g	D (cm^{-1})	B_4^0 (cm^{-1})	H_c (T)	U_{eff} (K)	E (K)	τ_0 (s)
2	1.92	−0.44	0.12×10^{-4}	0.340	53	63	7.4×10^{-9}
3	1.96	−0.40	0.24×10^{-4}	0.075	51	58	5.7×10^{-9}
4	2.06	−0.40	0.24×10^{-4}	0.046	51	58	6.0×10^{-9}
5				0.016	52		3.8×10^{-9}
6				0.0075	53		1.7×10^{-9}

Mn_{12} derivatives. The postulated spin Hamiltonian can be expressed in its simplest form by

$$\hat{\mathbf{H}} = -g\mu_B H\hat{\mathbf{S}} + D\left[\hat{S}_z^2 - \frac{1}{3}S(S+1)\right] \qquad (1)$$

where g is the effective Landé factor and D is the axial zero-field-splitting parameter. This Hamiltonian generally accounts for the thermodynamic properties of Mn_{12} derivatives. It has been shown, however, that the HF-EPR spectra of these complexes are best described considering the existence of higher order terms in the spin Hamiltonian,[18] like the quartic zero-field interaction term $B_4^0\hat{\mathbf{O}}_4^0$.[19] The complete spin Hamiltonian is then given by the following expression:

$$\hat{\mathbf{H}} = -g\mu_B H\hat{\mathbf{S}} + D\left[\hat{S}_z^2 - \frac{1}{3}S(S+1)\right] + B_4^0\hat{\mathbf{O}}_4^0 \qquad (2)$$

Here $\hat{\mathbf{O}}_4^0 = 35\hat{S}_z^4 - 30S(S+1)\hat{S}_z^2 + 25\hat{S}_z^2 - 6S(S+1)$. For an arbitrary set of ground-state spin S and magnetic parameters, the energy matrixes corresponding to eqs 1 and 2 can be diagonalized and the eigenvalues E_i can be used in eq 3 for the calculation of the magnetization of the different compounds.

$$M = N\sum_{i=1}^{P}\left(\frac{-\delta E_i}{\delta H}\right)\exp(-E_i/kT)/\sum_{i=1}^{P}\exp(-E_i/kT) \qquad (3)$$

The solid lines in Figure 9 represent least-squares fits of the seven isofield magnetization data sets recorded for **2**−**4**. The best-fit parameters of the different complexes are gathered in Table 2.

Magnetization hysteresis loops have been measured at 2 K for randomly oriented powder samples of the different salts **2**−**6**. A common feature in the magnetization curves is the fact that saturation is not reached in a 5 T field. This is in contrast with the situation found in most of the experiments that have been performed on single crystals or oriented microcrystalline samples and reflects the fact that the particles are not perfectly oriented with respect to the applied field. Table 2 lists the values of coercive field H_c for the different compounds. It is worth mentioning (Figure 10) that, in the Keggin series, the diamagnetic compound **4** has a higher coercive field than the paramagnetic Ni- and Co-containing

(18) (a) Barra, A.-L.; Gatteschi, D.; Sessoli, R. *Phys. Rev. B* **1997**, *56*, 8192. (b) Barra, A.-L.; Brunel, L.-C.; Gatteschi, D.; Pardi, L.; Sessoli, R. *Acc. Chem. Res.* **1998**, *31*, 460. (c) Artus, P.; Boskovic, C.; Yoo, J.; Streib, W. E.; Brunel, L.-C.; Hendrickson, D. N.; Christou, G. *Inorg. Chem.* **2001**, *40*, 4199.

(19) We have also performed a series of fittings with consideration of rhombic ZFS and quartic zero-field interactions term. However, the quality of the fit is not sensitive to the values of the corresponding E and B_4^4 parameters.

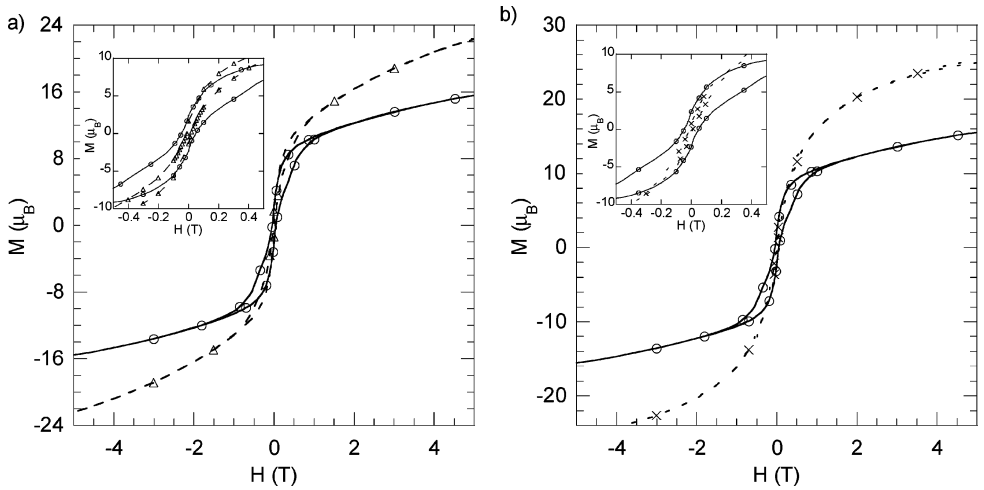

Figure 10. Magnetization hysteresis loops at 2 K of the Mn_{12} Keggin salt **4** (solid line) compared to the nickel(II)- (a) and the cobalt(II)-containing (b) polyoxometalate salts (dotted lines). The insets show the low-field regions of each plot.

(**5** and **6**) analogues. It is tempting to attribute this difference of behavior to an enhancement of the relaxation of the magnetization mediated by the presence of the paramagnetic anions, as has been claimed in a Mn_{12}-containing a cationic nitroxide free radical.[8] However, the shape of the hysteresis loop is always sensitive to the morphology of the sample and/or the presence of solvates and care should be taken with this kind of comparison when working with powdered samples. Further, in a recent report the effect of ferrocenium cations on the magnetic properties of salts of reduced $[Mn_{12}]^-$ derivatives has been considered to be negligibly small.[9]

Alternating Current Magnetic Susceptibility Studies. The observation of a frequency-dependent out-of-phase signal in the ac magnetic susceptibility measurements at zero dc field is indicative of SMM behavior and gives evidence on the dynamics of the relaxation of its magnetization. Below the blocking temperature, the magnetization is frozen in one of the potential wells of Figure 2, so that it cannot stay in phase with the oscillating applied magnetic field. A maximum in the out-of-phase (χ''_M) signal will take place when the frequency of the ac field matches the rate at which a molecule can interconvert between the two ground states of the potential energy curve. From magnetic measurements at different frequencies, it is possible to obtain the effective energy barrier for relaxation of the magnetization and an estimate of the zero-field-splitting parameter. Also, it is now established that two relaxation processes can be observed in the ac susceptibility study of Mn_{12} complexes: a high-temperature (HT) process that occurs in the 4−7 K range and a low-temperature (LT) process taking place in the 2−3 K range. This difference in the relaxation rates has been ascribed to the respective alignment of the Jahn−Teller axes of Mn^{III} ions in the system (Jahn−Teller isomerism).[20]

Ac magnetic susceptibility data were collected on powdered samples of **2**−**6** in the 2−10 K range under an applied oscillating field of 3.95 G at different frequencies. The external dc magnetic field was set to zero. Frequency-dependent out-of-phase signals were observed for all the compounds studied herein, indicating that the cationic Mn_{12} fragment retain its SMM character upon formation of the different salts. Figure 11 shows plots of $\chi'_M T$ and χ''_M versus temperature for complex **2**. Note that only one well-defined peak is observed for each frequency in the 3−5.5 K temperature range, indicating that the LT relaxation phase is not present in this sample. For salts **3**−**6**, the presence of a shoulder in the out-of-phase signal can be due to a significant amount of a "Jahn−Teller isomer" that shows LT relaxation. The shoulder is observed in all polyoxometalate salts irrespective of the nature of the anion (diamagnetic in **3** and **4**; paramagnetic in **5** and **6**). However, the intensity of this second signal is higher for samples **5** and **6** (Figure 12). Also, the Co-containing compound shows a stronger LT signal than the analogous nickel derivative. These two facts point to an enhancement of the relaxation mediated by the presence of the paramagnetic counteranions. In the absence of a structural characterization, however, it is difficult to discard the influence of the existence of several isomers and/or the morphology of the powder samples in the magnetic properties. In all cases, the HT out-of-phase signal can be extracted by fitting procedures assuming a Lorentzian shape. From the frequency dependence of the maximum of this signal, it is then possible to evaluate the effective energy barrier U_{eff} for magnetization reversal with the following equation:

$$\tau = \tau_0 \exp(+U_{eff}/kT) \qquad (4)$$

Here $\tau = 1/2\pi\nu$ is the relaxation time, ν is the operating frequency, k is the Boltzmann constant, and τ_0 is the preexponential factor, which is estimated along with U_{eff} by plotting the natural logarithm of the relaxation time versus the inverse of the temperature at the maximum. Table 2 lists values of τ_0 and U_{eff} parameters for **2**−**6**, together with the calculated values obtained from the expression $E = M_S^2 D$, using $M_S = \pm 10$ and the D values obtained from the magnetization curves. Clearly, all U_{eff} values are similar and

(20) (a) Sun, Z.; Ruiz, D.; Dilley, N. R.; Soler, M.; Ribas, J.; Folting, K.; Maple, M. B.; Christou, G.; Hendrickson, D. N. *Chem. Commun.* **1999**, 1973. (b) Aubin, S. M. J.; Sun, Z.; Eppley, H. J.; Rumberger, E. M.; Guzei, I. A.; Folting, K.; Gantzel, P. K.; Rheingold, A. L.; Christou, G.; Hendrickson, D. N. *Inorg. Chem.* **2001**, *40*, 2127.

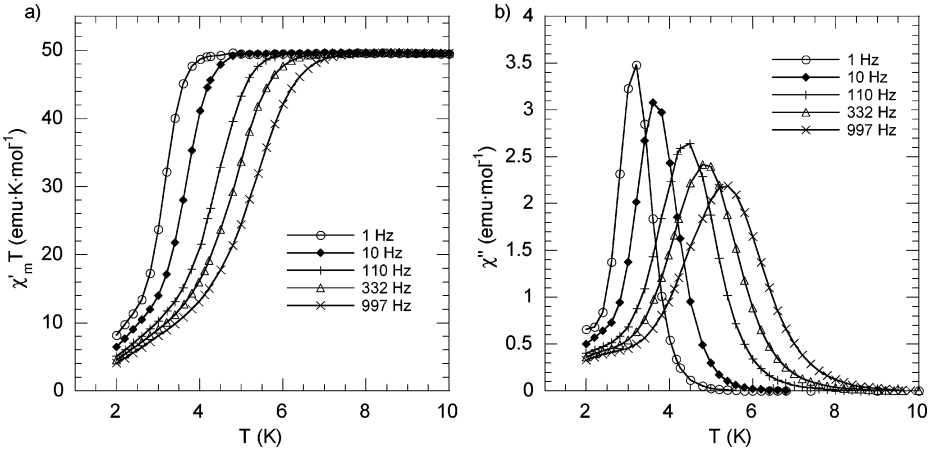

Figure 11. (a) Thermal variation of the product of the in-phase component of the ac molar magnetic susceptibility of **2** with temperature, at different frequencies. (b) Temperature dependence of the corresponding out-of-phase components.

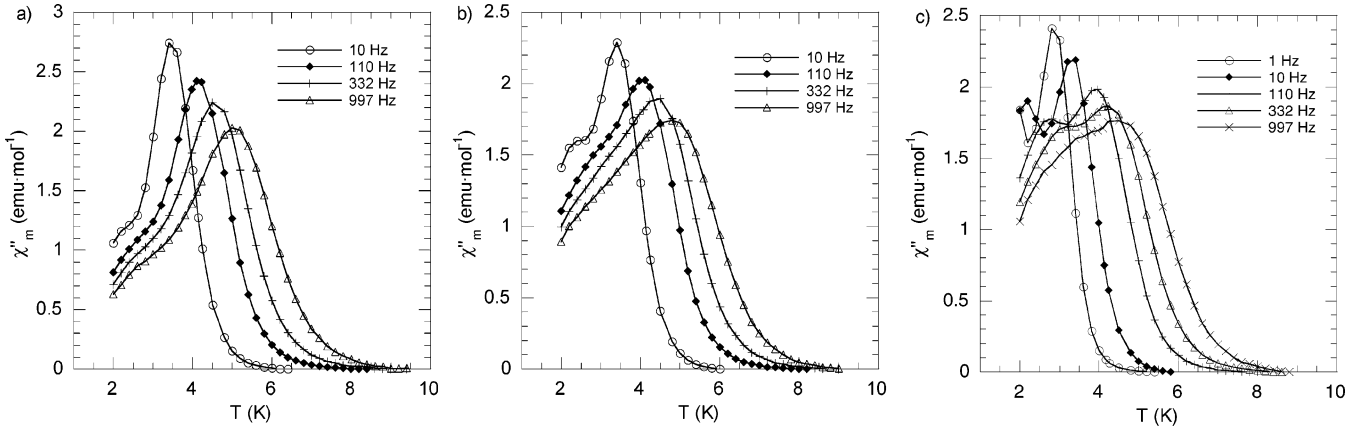

Figure 12. Temperature dependence of the out-of-phase components of **4** (a), **5** (b), and **6** (c) at different frequencies.

compare well with those reported for other Mn_{12} derivatives. Note, however, that the preexponential factors τ_o for the samples containing paramagnetic polyoxoanions are significantly lower than their diamagnetic counterparts. This explains the difference in relaxation rates of compounds having similar activation energies. In general, the effective energy barrier is smaller than that calculated for a pure thermally activated process ($U_{eff} < E$) as a consequence of the quantum tunneling of the magnetization.

Conclusion

The reaction of neutral $[Mn_{12}O_{12}(O_2CCH_3)_{16}(H_2O)_4]$ (**1**) with a carboxy-substituted tetraalkylammonium salt affords the polycationic single-molecule magnet **2**. This large molecule, with a molecular mass of 8355 Da and an estimated mean diameter of 35 Å, has been readily characterized by ES-MS. Mass spectrometry has then been added to the list of the different techniques used in the study of these interesting molecules. It has been shown that **2** forms stable salts with different diamagnetic and paramagnetic polyoxometalates. The resulting compounds retain their SMM character and constitute valuable models for the deposition of the polycationic Mn_{12} cluster onto metal oxide surfaces. Interestingly, the salts containing a paramagnetic polyoxometalate appear to exhibit higher relaxation rates than their diamagnetic counterparts. It remains an open question if this enhancement of the relaxation rate is due to the presence of the paramagnetic anions or the presence of different isomers in the systems. Also, the cationic SMM can be a useful precursor for the organization of the magnetic clusters in two dimensions by using the Langmuir−Blodgett technique. Studies to elucidate these points are in progress.

Acknowledgment. The authors are grateful for financial support from the European Union (TMR HPRN-CT-1999-00012) and the Spanish Ministerio de Ciencia y Tecnología (MCyT) (Project No. MAT2001-5408-E). F.M.R. thanks the MCyT for a research contract (Programa Ramón y Cajal). A.F.-A. thanks the Universitat de València for a predoctoral fellowship. Thanks are also extended to the SCIC of the University Jaume I for ESI-MS facilities and to Dr. Teresa Blasco (ITQ, UPV) for the MAS ^{31}P NMR measurements.

Supporting Information Available: Tables S1 and S2, listing peak assignments for the mass spectra shown in Figures 4−6, Figures S1 and S2, showing respectively the high-mass and low-mass regions of the ES-MS spectrum of the mixture obtained after the first treatment of **1** with an excess of **Z**HPF_6, Table S3, listing the corresponding peak values and assignments, and a summary of the different attempts to grow single crystals of compounds **2**−**6**. This material is available free of charge via the Internet at http://pubs.acs.org.

IC034407R